INTERNATIONAL JOURNAL FOR NUMERICAL METHODS IN FLUIDS
Int. J. Numer. Meth. Fluids 2007; **54**:1425–1450
Published online 25 January 2007 in Wiley InterScience (www.interscience.wiley.com). DOI: 10.1002/fld.1428

A numerical method for one-dimensional compressible multiphase flows on moving meshes

Richard Saurel[1, 2, *, †], Jacques Massoni[1] and François Renaud[3]

[1]*Polytech Marseille, Projet SMASH UMR CNRS 6595-IUSTI-INRIA, 5 rue E. Fermi, 13453 Marseille Cedex 13, France*
[2]*University Institute of France, 5 rue E. Fermi, 13453 Marseille Cedex 13, France*
[3]*CEA/DIF, DCSA/SSEL, BP 12, 91680 Bruyères le Châtel, France*

SUMMARY

This paper is devoted to the numerical approximation of a hyperbolic non-equilibrium multiphase flow model with different velocities on moving meshes. Such goal poses several difficulties. The presence of different flow velocities in conjunction with cell velocities poses difficulties for upwinding fluxes. Another issue is related to the presence of non-conservative terms. To solve these difficulties, the discrete equations method (*J. Comput. Phys.* 2003; **186**(2):361–396; *J. Fluid. Mech.* 2003; **495**:283–321; *J. Comput. Phys.* 2004; **196**:490–538; *J. Comput. Phys.* 2005; **205**:567–610) is employed and generalized to the context of moving cells. The complementary conservation laws, available for the mixture, are used to determine the velocities of the cells boundaries. With these extensions, an accurate and robust multiphase flow method on moving meshes is obtained and validated over several test problems with exact or experimental solutions. Copyright © 2007 John Wiley & Sons, Ltd.

Received 13 December 2005; Revised 21 November 2006; Accepted 24 November 2006

KEY WORDS: multiphase flows; hyperbolic models; Riemann problem; Lagrangian hydrocodes

1. INTRODUCTION

Compressible multiphase flow with several velocities has important fundamental and industrial applications. Some of them deal with high-speed flows, such as shock and detonation waves through mixtures of materials or the turbulent mixing of compressible fluids, as well as mixtures of plasmas in astrophysics. In these domains, Lagrangian methods are often preferred to Eulerian ones because of their lower diffusion properties at material interfaces and their ability to couple domains of different physics.

*Correspondence to: Richard Saurel, Polytech Marseille, Projet SMASH UMR CNRS 6595-IUSTI-INRIA, 5 rue E. Fermi, 13453 Marseille Cedex 13, France.
†E-mail: richard.saurel@polytech.univ-mrs.fr

High-pressure conditions involved in these flows require compressible effects consideration for all phases. Accounting for compressible effects also allows the determination of multiphase flow models that are unconditionally hyperbolic. Consequently, they are able to propagate correctly the various waves. Such type of models have been derived by Stewart and Wendroff [1], Baer and Nunziato [2], Youngs [3, 4], Kapila *et al.* [5], Saurel and Abgrall [6], Glimm *et al.* [7], Kapila *et al.* [8], Saurel and Metayer [9] and Gavrilyuk and Saurel [10]. The keypoint of these models relies in the differential expression of the pressure equilibrium condition. It is expressed by an extra evolution equation for the volume fraction including relaxation terms. These terms control the rate at which pressure equilibrium is reached after waves propagation.

The numerical approximation of these models is a difficult task. They contain non-conservative terms and many types of waves. In fact, up to seven waves are present: a set of two acoustic waves and a contact discontinuity are present for each fluid, supplemented by a volume fraction wave propagating at the average interface velocity. Such wave pattern complexifies fluxes computation. Moreover, the presence of non-conservative terms poses difficulties in the presence of shocks. To solve these difficulties, a new homogenization method has been developed recently and named 'discrete equations method (DEM)' [11–14]. This method is not only a homogenization method but is in fact a numerical method that applies the fundamental ideas of the Godunov method to a two-phase control volume. It consists in solving for each two-phase control volume, at its boundaries and at its internal interfaces, an initial value problem between the various fluids and states. The solution of these interface problems is obtained with the help of Riemann solvers for the Euler equations. Indeed, each pure fluid is governed by the Euler equations. All Riemann problem solutions are then averaged over the phases control volumes, in a similar way as done with the Euler equations and the Godunov scheme. The result is a set of discrete equations that describes the two-phase mixture involving interaction terms. These discrete equations correspond to a numerical scheme.

The aim of the present paper is the extension of the DEM method to moving meshes. To this end, we follow the same methodology and give particular attention to the Lagrangian case. Indeed, a lot of research and industrial codes related to high-energy flows use Lagrangian methods with reduced numerical diffusion of convective waves [15–20]. The development of such method in the present two-phase flows context poses extra difficulties related to the approximation of non-conservative terms over moving meshes, the upwinding of the various fluxes, as well as the determination of the cell boundary velocities. Indeed four velocities are present: the two averaged fluid velocities, the average interface velocity and the cell boundaries velocities.

The paper is organized as follows. We present the theoretical models we are dealing with in Section 2. In Section 3 we recall the DEM for Eulerian computations. In Section 4 we extend the DEM for moving meshes. In Section 5 we detail the way the cell boundary velocity is obtained. In Section 6 the method is validated *versus* test problems with exact or experimental solutions.

2. TWO-PHASE FLOW MODEL

The mixture contains two phases with indexes 1 and 2. Each phase k is compressible and obeys an appropriate equation of state $P_k = P_k(\rho_k, \mathrm{e}_k)$ where P, ρ and e denote, respectively, the pressure, density and specific internal energy. Governing equations (1) correspond to a system of seven partial differential equations. We present the system for the phase 1 only, the equations being

DOI: 10.1002/fld

perfectly symmetric for phase 2

$$\begin{aligned}
\frac{\partial \alpha_1}{\partial t} + u_\mathrm{I}\frac{\partial \alpha_1}{\partial x} &= \mu(P_1 - P_2)\\
\frac{\partial \alpha_1\rho_1}{\partial t} + \frac{\partial(\alpha_1\rho_1 u_1)}{\partial x} &= 0\\
\frac{\partial \alpha_1\rho_1 u_1}{\partial t} + \frac{\partial(\alpha_1\rho_1 u_1^2 + \alpha_1 P_1)}{\partial x} &= P_\mathrm{I}\frac{\partial \alpha_1}{\partial x} + \lambda(u_2 - u_1)\\
\frac{\partial \alpha_1\rho_1 E_1}{\partial t} + \frac{\partial(\alpha_1\rho_1 E_1 u_1 + \alpha_1 P_1 u_1)}{\partial x} &= P_\mathrm{I} u_\mathrm{I}\frac{\partial \alpha_1}{\partial x} - \mu P'_\mathrm{I}(P_1 - P_2) + \lambda u'_\mathrm{I}(u_2 - u_1)
\end{aligned} \tag{1}$$

with

$$P_\mathrm{I} = \frac{Z_1 P_2 + Z_2 P_1}{Z_1 + Z_2} + \mathrm{sgn}\left(\frac{\partial \alpha_1}{\partial x}\right)\frac{(u_2 - u_1)Z_1 Z_2}{Z_1 + Z_2}$$

$$P'_\mathrm{I} = \frac{Z_1 P_2 + Z_2 P_1}{Z_1 + Z_2}$$

$$u_\mathrm{I} = \frac{Z_1 u_1 + Z_2 u_2}{Z_1 + Z_2} + \mathrm{sgn}\left(\frac{\partial \alpha_1}{\partial x}\right)\frac{P_2 - P_1}{Z_1 + Z_2}$$

$$u'_\mathrm{I} = \frac{Z_1 u_1 + Z_2 u_2}{Z_1 + Z_2}$$

$$\mu = \frac{S}{Z_1 + Z_2}, \quad \lambda = \mu Z_1 Z_2$$

The first equation expresses the evolution of the phase 1 volume fraction α_1. It propagates with the average interface velocity u_I, whose expression has been determined in [12]. During propagation, the volume fraction varies according to the pressure differential $(P_1 - P_2)$. The volume variation rate is controlled by the relaxation parameter μ. Its expression has been determined in the same reference and depends on the specific surface S and the phases acoustic impedances $Z_k = \rho_k c_k$, where c_k represents the phase k sound speed.

The second equation represents the phase 1 mass conservation. The third one expresses the evolution of momentum. A non-conservative term is present on the right-hand side with the average of the interface pressure P_I. The pressure drag force term $\lambda(u_2 - u_1)$ is responsible for velocities relaxation, which occurs at a rate controlled by λ. Its expression shows a direct connection to the pressure relaxation parameter μ.

The last equation corresponds to the evolution of the specific total energy (defined by $E_1 = \mathrm{e}_1 + 1/2u_1^2$) of phase 1. The interfacial pressure work occurring during the pressure relaxation process appears in term $-\mu P'_\mathrm{I}(P_1 - P_2)$ and involves the volume average interface pressure P'_I given above. The pressure drag force work also involves a volume average interface velocity u'_I. The non-trivial expressions for all these interface variables P_I, P'_I, u_I, u'_I as well as for the relaxation parameters λ and μ are demonstrated and explained in Saurel *et al.* [12] and Chinnayya *et al.* [13]. In particular, the velocity relaxation parameter is valid for inviscid fluid mixtures. When dealing with dissipative fluids, the drag coefficient has to be complemented by viscous effects.

DOI: 10.1002/fld

This system forms a non-conservative set of equations, unconditionally hyperbolic. It can be easily shown that it involves seven characteristic wave speeds: $\lambda_0^1 = u_1$; $\lambda_1^1 = u_1 - c_1$; $\lambda_2^1 = u_1 + c_1$; $\lambda_0^2 = u_2$; $\lambda_1^2 = u_2 - c_2$; $\lambda_2^2 = u_2 + c_2$ and $\lambda_I = u_I$.

The derivation of a Lagrangian numerical scheme for the model (1) is the aim of this paper. Such goal will be reached by extending the DEM. This method being quite unconventional, its basic ingredients are recalled in the context of motionless Eulerian cells in the next section.

3. RECALLS OF THE DISCRETE EQUATIONS METHOD (DEM) FOR EULERIAN MESHES

The DEM is a variant of averaging methods described, for example, in Drew and Passman [21]. With conventional averaging method, each pure fluid is governed by a continuum mechanics flow model that is selected and averaged with the help of a phase function. Such systems are usually non-conservative and need non-trivial closure relations. With these conventional approaches, the next step is to integrate numerically over space and time the partial differential equation (PDE) system. This poses a supplementary problem related to the numerical approximation of the non-conservative terms. An example of these difficulties is given in Hou and Floch [22] and Dalmaso *et al.* [23], and a partial solution is given in Saurel and Abgrall [6].

With the DEM we proceed in the opposite way to what is usually done. The pure fluid equations solutions are computed at the scale of each inclusion and these solutions are averaged over the various fluids volumes inside the computational cell. This method is due to Abgrall and Saurel [11] and has been developed for the numerical approximation of the 7 equation model (1). To be more precise, with the DEM, the pure phase conservation laws are considered at the microscopic level. The Riemann problem of the Euler equations is solved for each initial value problem present at each cell boundary and inside the control volume where inner interfaces are present. These solutions are then averaged over the control volume and provide the corresponding numerical scheme for the averaged multiphase flow equations. The method provides the numerical scheme and contains implicitly the correct averages of interfacial pressure, velocity as well as relaxation terms.

The first step with the DEM is to give the topology of the two-phase mixture. We have shown in [12, 13] that the numerical approximations of the fluxes as well as non-conservative terms are not dependent on this flow topology. Only the relaxation part of the model is strongly dependent of the flow topology. Thanks to this remark, we consider the representation of a separated multiphase mixture, namely an annular two-phase flow as represented in Figure 1.

We consider a computational mesh $x_i (i \in Z)$ and the associated control volumes $C_i =]x_{i-1/2}, x_{i+1/2}[\times]0, H[$ where $x_{i+1/2} = (x_i + x_{i+1})/2$ and H represents the height of the tube section. The flow involves two non-miscible phases 1 and 2. The two-phase mixture at the cell scale may be approximated by three horizontal layers separated by an interface as shown in Figure 1.

Since this geometrical configuration is two dimensional, each pure fluid obeys the two-dimensional Euler equations:

$$\frac{\partial U}{\partial t} + \frac{\partial F}{\partial x} + \frac{\partial G}{\partial y} = 0 \tag{2}$$

DOI: 10.1002/fld

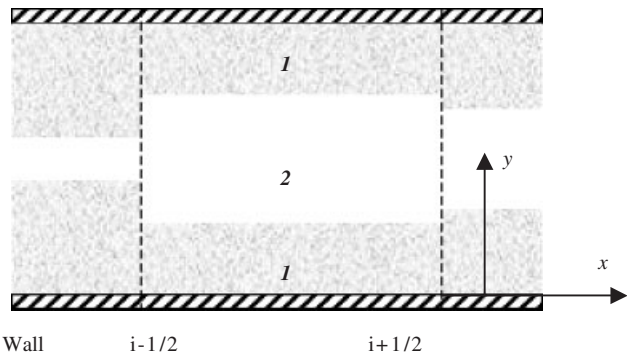

Figure 1. Schematic representation of a computational cell consisting of three horizontal fluid layers.

where $U=[1, \rho, \rho u, \rho v, \rho E]^{\mathrm{T}}$, $F=[0, \rho u, \rho u^2+P, \rho uv, (\rho E+P)u]^{\mathrm{T}}$ and $G=[0, \rho v, \rho uv, \rho v^2+P, (\rho E+P)v]^{\mathrm{T}}$.

The first trivial equation $\partial 1/\partial t+\partial 0/\partial x+\partial 0/\partial y=0$ comes from an evolution equation expressing the link between the Lagrangian and Eulerian coordinates. This trivial identity will be necessary to obtain the volume fraction numerical scheme.

To obtain the local equations of each pure fluid k, we multiply the Euler equations (2) by the phase function X_k of each fluid. This one only admits two values: $X_k(M,t)=1$ if the point M is located in the phase k at time t and $X_k(M,t)=0$ otherwise. This function obeys the local evolution equation:

$$\frac{\partial X_k}{\partial t}+\sigma_x\frac{\partial X_k}{\partial x}+\sigma_y\frac{\partial X_k}{\partial y}=0 \tag{3}$$

where σ_x and σ_y are the components of the local interface velocity.

After some algebraic manipulations, the local pure fluids equations are given by

$$\frac{\partial X_k U}{\partial t}+\frac{\partial X_k F}{\partial x}+\frac{\partial X_k G}{\partial y}=F^{\mathrm{lag}}\frac{\partial X_k}{\partial x}+G^{\mathrm{lag}}\frac{\partial X_k}{\partial y} \tag{4}$$

where the Lagrangian fluxes are defined as $F^{\mathrm{lag}}=F-\sigma_x U$ and $G^{\mathrm{lag}}=G-\sigma_y U$.

These Lagrangian fluxes are used only at the interfaces separating the various phases. At these interfaces, in absence of mass transfer we have $\sigma_x=u$ and $\sigma_y=v$. In this case, the Lagrangian fluxes read $F^{\mathrm{lag}}=[-u, 0, P, 0, Pu]^{\mathrm{T}}$ and $G^{\mathrm{lag}}=[-v, 0, 0, P, Pv]^{\mathrm{T}}$.

The next step consists in the integration over time and space of Equation (4):

$$\int_0^{\Delta t}\int_{C_i}\left(\frac{\partial X_k U}{\partial t}+\frac{\partial X_k F}{\partial x}+\frac{\partial X_k G}{\partial y}\right)\mathrm{d}V\,\mathrm{d}t=\int_0^{\Delta t}\int_{C_i}\left(F^{\mathrm{lag}}\frac{\partial X_k}{\partial x}+G^{\mathrm{lag}}\frac{\partial X_k}{\partial y}\right)\mathrm{d}V\,\mathrm{d}t \tag{5}$$

Relation (5) can be written as

$$I_1+I_2+I_3=I_4+I_5 \tag{6}$$

DOI: 10.1002/fld

with

$$I_1 = \int_0^{\Delta t}\int_{C_i} \frac{\partial X_k U}{\partial t}\,\mathrm{d}V\,\mathrm{d}t$$

$$I_2 = \int_0^{\Delta t}\int_{C_i} \frac{\partial X_k F}{\partial x}\,\mathrm{d}V\,\mathrm{d}t, \quad I_3 = \int_0^{\Delta t}\int_{C_i} \frac{\partial X_k G}{\partial y}\,\mathrm{d}V\,\mathrm{d}t$$

$$I_4 = \int_0^{\Delta t}\int_{C_i} F^{\mathrm{lag}}\frac{\partial X_k}{\partial x}\,\mathrm{d}V\,\mathrm{d}t, \quad I_5 = \int_0^{\Delta t}\int_{C_i} G^{\mathrm{lag}}\frac{\partial X_k}{\partial y}\,\mathrm{d}V\,\mathrm{d}t$$

Now, these five integrals have to be computed in order to obtain the discrete macroscopic equations of each fluid.

To this end, we define the following averaging operators:

$$\begin{aligned}
&\text{Volume average: } \langle f\rangle = \frac{1}{V}\int_V f\,\mathrm{d}V\\
&\text{Surface averages: } \widehat{f} = \frac{1}{\Delta x}\int_{x_{i-1/2}}^{x_{i+1/2}} f\,\mathrm{d}x, \quad \bar{f} = \frac{1}{H}\int_0^H f\,\mathrm{d}y\\
&\text{Time average: } \widetilde{f} = \frac{1}{\Delta t}\int_0^{\Delta t} f\,\mathrm{d}t\\
&\text{Phase average: } \{f_k\} = \frac{1}{V_k}\int_V X_k U\,\mathrm{d}V = \frac{1}{V_k}\int_{V_k} U_k\,\mathrm{d}V
\end{aligned} \tag{7}$$

3.1. *Integration of the temporal term* I_1

The first integral I_1 reads

$$I_1 = \int_0^{\Delta t}\int_{C_i} \frac{\partial X_k U}{\partial t}\,\mathrm{d}V\,\mathrm{d}t = \int_{C_i} (X_k U)^{n+1}\,\mathrm{d}V - \int_{C_i} (X_k U)^n\,\mathrm{d}V = \left(\langle X_k U\rangle_i^{n+1} - \langle X_k U\rangle_i^n\right) V_i$$

Using the volume average of the phase function X_k in the cell C_i, we have

$$\langle X_k\rangle_i = \frac{1}{V_i}\int_{C_i} X_k\,\mathrm{d}V = \frac{V_{k,i}}{V_i} \stackrel{\mathrm{def}}{=} \alpha_{k,i}$$

where $V_{k,i}$ represents the volume occupied by the phase k in the cell C_i.

Then, the term I_1 reads

$$I_1 = ((\alpha_k\{U_k\})_i^{n+1} - (\alpha_k\{U_k\})_i^n) V_i$$

where $\{U_k\}_i \stackrel{\mathrm{def}}{=} (1/V_{k,i})\int_{C_{k,i}} U_k\,\mathrm{d}V$ is the phase average of U_k in $V_{k,i}$.

DOI: 10.1002/fld

3.2. *Integration of the convective fluxes I_2 and I_3*

The second integral I_2 reads

$$I_2 = \int_0^{\Delta t}\int_{C_i} \frac{\partial X_k F}{\partial x}\,\mathrm{d}V\,\mathrm{d}t = \int_0^{\Delta t}\int_0^{H} (X_k F)_{i+1/2}\,\mathrm{d}y\,\mathrm{d}t - \int_0^{\Delta t}\int_0^{H} (X_k F)_{i-1/2}\,\mathrm{d}y\,\mathrm{d}t$$

Using the previous averages, we obtain

$$I_2 = H\int_0^{\Delta t} (\overline{X_k F})_{i+1/2}\,\mathrm{d}t - H\int_0^{\Delta t} (\overline{X_k F})_{i-1/2}\,\mathrm{d}t = \Delta t H((\widetilde{\overline{X_k F}})_{i+1/2} - (\widetilde{\overline{X_k F}})_{i-1/2})$$

In order to determine the average Eulerian flux $\widetilde{\overline{X_k F}}$ at each cell boundary, we first compute the following surface averages:

$$\int_0^{H} (X_k F)_{i\pm 1/2}\,\mathrm{d}y = \sum_{l,m} (S X_k^* F^*)_{lm,i\pm 1/2}$$

where S_{lm} represents the contact surface for each pair of fluids in contact.

Consider the cell boundary $(i-1/2)$ shown in Figure 1. The various types of contacts at this cell boundary and for this specific flow configuration are schematized in the Figure 2. Let us denote by (l, m) the configuration where the fluid l is present on the left and the fluid m is present on the right at a given cell boundary. In the context of two fluids, four types of contact between pure fluids are possible at each cell boundary. For example, $S_{12,i-1/2}$ represents the contact surface at cell boundary $(i-1/2)$ between fluid 1 on the left (present in the cell C_{i-1}) and fluid 2 on the right (present in the cell C_i) (Figure 2). Each type of contact is associated with the corresponding surface $S_{lm,i-1/2}$. At each contact (l, m), the corresponding Riemann problem is solved. Its solution is denoted by the superscript '$*$' and is used for the computation of the various fluxes (Eulerian and Lagrangian). $X^*_{k,lm}$ represents the phase function of fluid k for the same pair. Its value is reported in Table I and is obtained from the Riemann problem solution, according to the location of fluid k.

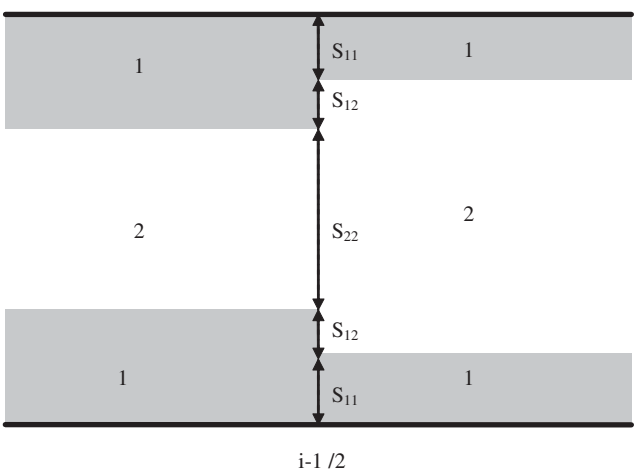

Figure 2. Schematic representation of the different types of contact at a cell boundary.

DOI: 10.1002/fld

Table I. The different configurations for Eulerian fluxes at cell boundary $(i-1/2)$ for fluid $k=1$.

Contact	Surface	Eulerian flux	Phase function X_1^*
1–1	$S_{11}=H\,\mathrm{Min}(\alpha_{1,i-1},\alpha_{1,i})$	F_{11}^*	$X_{1,11}^*=1$
1–2	$S_{12}=H\,\mathrm{Max}(0,\alpha_{1,i-1}-\alpha_{1,i})$	F_{12}^*	$X_{1,12}^*=\begin{cases}1 & \text{if } u_{12}^*>0\\ 0 & \text{otherwise}\end{cases}$
2–1	$S_{21}=H\,\mathrm{Max}(0,\alpha_{1,i}-\alpha_{1,i-1})$	F_{21}^*	$X_{1,21}^*=\begin{cases}1 & \text{if } u_{21}^*<0\\ 0 & \text{otherwise}\end{cases}$
2–2	$S_{22}=H\,\mathrm{Min}(\alpha_{2,i-1},\alpha_{2,i})$	F_{22}^*	$X_{1,22}^*=0$

The contact surfaces, reported also in Table I for cell boundary $(i-1/2)$, are obtained following simple geometrical arguments. Consider, for example, contact (1, 1). The height of contact corresponds to the minimum of the two levels/heights of fluid 1 on both sides. Thus, the length of contact is $H\,\mathrm{Min}(\alpha_{1,i-1};\alpha_{1,i})$. The indicator function X_1 is always equal to 1 for this type of contact. The flux that crosses the cell boundary along this height is solution of the Riemann problem of the Euler equations with fluid 1 of cell $(i-1)$ on the left and fluid 1 of cell (i) on the right.

On another part of cell boundary $(i-1/2)$, fluid 1 on the left is in contact with fluid 2 on the right. In such instance, the length of contact is $H(\alpha_{1,i-1}-\alpha_{1,i})$. Such type of contact appears only when the level of fluid 1 in cell $(i-1)$ is higher than the one of cell (i). In order to consider in a single formulae the situation when the level of fluid 1 in cell $(i-1)$ is lower than the one in cell (i), the height of contact is given by the general formulae $H\,\mathrm{Max}(0;\alpha_{1,i-1}-\alpha_{1,i})$. We also have to determine the indicator function for this contact at the cell boundary. The interface between 1 and 2 may enter cell (i) or leave it. When it enters the cell $(u^*(1,2)>0)$, the convective fluxes must be accounted for in the evolution of fluid 1. The corresponding flux is solution of the Riemann problem of the Euler equations with fluid 1 on the left and fluid 2 on the right.

The remaining contacts (2, 1) and (2, 2) are treated identically as summarized in Table I.

When fluid k is present on both sides of the interface, $X_k^*=1$. When the other fluid is present on both sides, $X_k^*=0$. These situations correspond to the first and last lines of the Table I, respectively.

As the Riemann problem is solved to determine the contact discontinuity velocity u_{lm}^*, the whole solution is sampled along the axis $x/t=0$ and allows the various fluxes computation F_{lm}^*.

The Eulerian fluxes are supposed to be constant during a time step (CFL condition), thus we have

$$I_2=\Delta t\left(\sum_{l,m}\left(SX_k^*F^*\right)_{lm,i+1/2}-\sum_{l,m}\left(SX_k^*F^*\right)_{lm,i-1/2}\right)$$

The third integral I_3 is obtained as previously:

$$I_3=\int_0^{\Delta t}\int_{C_i}\frac{\partial X_kG}{\partial y}\,\mathrm{d}V\,\mathrm{d}t=\Delta t\Delta x((\widetilde{\widetilde{X_kG}})_{j+1/2}-(\widetilde{\widetilde{X_kG}})_{j-1/2})$$

DOI: 10.1002/fld

Due to the wall boundary conditions and symmetry of the annular flow topology, this integral vanishes:

$$I_3 = 0$$

3.3. *Integration of the non-conservative terms I_4 and I_5*

The fourth integral I_4 involves the Lagrangian fluxes. It reads

$$I_4 = \int_0^{\Delta t}\int_{C_i} F^{\text{lag}} \frac{\partial X_k}{\partial x}\,\mathrm{d}V\,\mathrm{d}t = \int_0^{\Delta t}\int_0^{H}\int_{x_{i-1/2}}^{x_{i+1/2}} F^{\text{lag}} \frac{\partial X_k}{\partial x}\,\mathrm{d}x\,\mathrm{d}y\,\mathrm{d}t$$

The only interfaces present in the flow topology considered in Figure 1 where $\partial X_k/\partial x$ in non-zero are located at the cell boundaries. Then, I_4 reads

$$I_4 = \int_0^{\Delta t}\int_0^{H} \left(F^{\text{lag}}[X_k^x]\right)_{i-1/2}\,\mathrm{d}y\,\mathrm{d}t + \int_0^{\Delta t}\int_0^{H} (F^{\text{lag}}[X_k^x])_{i+1/2}\,\mathrm{d}y\,\mathrm{d}t$$

where $[X_k^x]$ represents the jump of X_k in the x-direction through an interface. As detailed in Abgrall and Saurel [11], the preceding integration is allowed because the Lagrangian flux F^{lag} is uniform at every location where $\partial X_k/\partial x$ is non-zero.

By using the definitions of averages, we obtain

$$I_4 = \Delta t\, H((\widetilde{F^{\text{lag}}[X_k^x]})_{i-1/2} + (\widetilde{F^{\text{lag}}[X_k^x]})_{i+1/2})$$

As for the calculations of the Eulerian fluxes, we use the considerations described in Table II (for cell boundary $(i-\frac{1}{2})$).

By summing the different terms, we obtain

$$\int_0^{H} (F^{\text{lag}}[X_k^x])_{i-1/2}\,\mathrm{d}y = \sum_{l,m} (SF^{\text{lag},*}[X_k^{x,*}])_{lm,i-1/2}$$

The jump of the phase function is zero when the same fluid is present on both sides of the interface (lines 1 and 4 of Table II). When the fluid under interest lies initially on the left and is entering

Table II. The different configurations for Lagrangian fluxes at cell boundary $(i-1/2)$ for fluid $k=1$.

Contact	Surface	Lagrangian flux	Jump $[X_1^x]^*$
1–1	S_{11}	$F_{11}^{\text{lag},*}$	$[X_1^x]_{11}^* = 0$
1–2	S_{12}	$F_{12}^{\text{lag},*}$	$[X_1^x]_{12}^* = \begin{cases} -1 & \text{if } u_{12}^* > 0 \\ 0 & \text{otherwise} \end{cases}$
2–1	S_{21}	$F_{21}^{\text{lag},*}$	$[X_1^x]_{21}^* = \begin{cases} 1 & \text{if } u_{21}^* > 0 \\ 0 & \text{otherwise} \end{cases}$
2–2	S_{22}	$F_{22}^{\text{lag},*}$	$[X_1^x]_{22}^* = 0$

DOI: 10.1002/fld

the cell (line 2 of Table II), the jump of its associated phase function is -1. When the considered fluid lies on the right and the other fluid is entering the cell (line 3 of Table II), the jump of its phase function is 1. The Lagrangian fluxes, in each type of contact, involve only the corresponding interface velocity and pressure that are provided by the Riemann solver.

For cell boundary $(i+1/2)$, we also have

$$\int_0^H (F^{\text{lag}}[X_k^x])_{i+1/2}\,\mathrm{d}y = \sum_{l,m} (SF^{\text{lag},*}[X_k^{x,*}])_{lm,i+1/2}$$

Assuming that the Lagrangian fluxes are constant during the time step, we have

$$I_4 = \Delta t \left(\sum_{l,m} (SF^{\text{lag},*}[X_k^{x,*}])_{lm,i-1/2} + \sum_{l,m} (SF^{\text{lag},*}[X_k^{x,*}])_{lm,i+1/2} \right)$$

The last integral I_5 is obtained similarly:

$$I_5 = \int_0^{\Delta t} \int_{C_i} G^{\text{lag}} \frac{\partial X_k}{\partial y}\,\mathrm{d}V\,\mathrm{d}t$$

The jump $[X_k]$ is non-zero only for the horizontal interfaces (see Figure 1) and the contact surface between phases reduces to the cell size. Consequently,

$$I_5^{(1)} = \Delta t \Delta x (G_i^{\text{lag},*}(2,1) - G_i^{\text{lag},*}(1,2))$$

$$I_5^{(2)} = -\Delta t \Delta x (G_i^{\text{lag},*}(2,1) - G_i^{\text{lag},*}(1,2))$$

where the superscripts denote the phase index.

The Lagrangian flux along the y-direction reads: $G^{\text{lag}} = (-v, 0, 0, P, Pv)^{\mathrm{T}}$. In the present one-dimensional context $v = 0\,\mathrm{m/s}$, but the pressures P_k are different in each fluid. It implies that the interface pressures are equal $P_i^*(1,2) = P_i^*(2,1)$ while the interface velocities are opposite. Thus, only the first and last components of I_5 are non-zero. We will show hereafter that this term does not involve any derivative. It represents a relaxation term.

Finally, numerical scheme (6) reads, for each fluid k:

$$\frac{(\alpha_k\{U_k\})_i^{n+1} - (\alpha_k\{U_k\})_i^n}{\Delta t} + \frac{(\widetilde{\overline{X_k F}})_{i+1/2} - (\widetilde{\overline{X_k F}})_{i-1/2}}{\Delta x}$$

$$= \frac{(\widetilde{\overline{F^{\text{lag}}[X_k^x]}})_{i-1/2} + (\widetilde{\overline{F^{\text{lag}}[X_k^x]}})_{i+1/2}}{\Delta x} + \frac{(G_i^{\text{lag},*}(k',k) - G_i^{\text{lag},*}(k,k'))}{H} \tag{8}$$

where all terms have been divided by $\Delta x H \Delta t$ and with

$$(\widetilde{\overline{X_k F}})_{i\pm1/2} = \frac{1}{H} \sum_{l,m} (SX_k^* F^*)_{lm,i\pm1/2}$$

$$(\widetilde{\overline{F^{\text{lag}}[X_k^x]}})_{i\pm1/2} = \frac{1}{H} \sum_{l,m} (SF^{\text{lag},*}[X_k^{x,*}])_{lm,i\pm1/2}$$

The ingredients involved in the computation of these two sums are given in Tables I and II.

DOI: 10.1002/fld

4. THE DISCRETE EQUATION METHOD FOR MOVING MESHES

The time-dependent two-phase control volume C_i corresponds to the computational cell: $C_i =]x_{i-1/2}, x_{i+1/2}[\times]0, H[$. Top and bottom boundaries, located at $y=0$ and $y=H$, respectively, are motionless. The right and left cell boundaries located at $x_{i+1/2}$ and $x_{i-1/2}$ are considered mobile since we are looking for an arbitrary Lagrangian Eulerian (ALE) or Lagrangian scheme. These boundaries are moving with the velocities $\dot{x}_{i+1/2}$ and $\dot{x}_{i-1/2}$, respectively. We will address the question of the determination of these velocities in a later section. With these definitions Equation (5) becomes

$$\int_0^{\Delta t} \frac{\mathrm{d}}{\mathrm{d}t} \int_{C_i(t)} (X_k U)\,\mathrm{d}x\,\mathrm{d}y\,\mathrm{d}t - \int_0^{\Delta t}\int_0^H ((\dot{x} X_k U)_{i+1/2} - (\dot{x} X_k U)_{i-1/2})\,\mathrm{d}y\,\mathrm{d}t$$
$$+ \int_0^{\Delta t}\int_0^H ((X_k F)_{i+1/2} - (X_k F)_{i-1/2})\,\mathrm{d}y\,\mathrm{d}t + \int_0^{\Delta t}\int_{x_{i-1/2}}^{x_{i+1/2}} ((X_k G)_{y=H} - (X_k G)_{y=0})\,\mathrm{d}x\,\mathrm{d}t$$
$$= \int_0^{\Delta t}\int_{C_i(t)} (F - \sigma_x U)\frac{\partial X_k}{\partial x}\,\mathrm{d}x\,\mathrm{d}y\,\mathrm{d}t + \int_0^{\Delta t}\int_{C_i(t)} (G - \sigma_y U)\frac{\partial X_k}{\partial y}\,\mathrm{d}x\,\mathrm{d}y\,\mathrm{d}t \tag{9}$$

The numerical scheme building consists in the approximation of the five integrals:

$$I_1 = \int_0^{\Delta t} \frac{\mathrm{d}}{\mathrm{d}t} \int_{C_i(t)} (X_k U)\,\mathrm{d}x\,\mathrm{d}y\,\mathrm{d}t$$

$$I_2 = \int_0^{\Delta t}\int_0^H ((X_k(F - \dot{x}U))_{i+1/2} - (X_k(F - \dot{x}U))_{i-1/2})\,\mathrm{d}y\,\mathrm{d}t$$

$$I_3 = \int_0^{\Delta t}\int_{x_{i-1/2}}^{x_{i+1/2}} ((X_k G)_{y=H} - (X_k G)_{y=0})\,\mathrm{d}x\,\mathrm{d}t$$

$$I_4 = \int_0^{\Delta t}\int_{C_i(t)} (F - \sigma_x U)\frac{\partial X_k}{\partial x}\,\mathrm{d}x\,\mathrm{d}y\,\mathrm{d}t$$

$$I_5 = \int_0^{\Delta t}\int_{C_i(t)} (G - \sigma_y U)\frac{\partial X_k}{\partial y}\,\mathrm{d}x\,\mathrm{d}y\,\mathrm{d}t$$

4.1. Approximation of the temporal term

The time integral reads

$$I_1 = \int_0^{\Delta t} \frac{\mathrm{d}}{\mathrm{d}t} \int_{C_i(t)} (X_k U)\,\mathrm{d}x\,\mathrm{d}y\,\mathrm{d}t = \int_0^{\Delta t} \frac{\mathrm{d}}{\mathrm{d}t} (\Delta x H(\alpha\{U_k\})_i\,\mathrm{d}t = H((\alpha\Delta x\{U_k\})_i^{n+1} - (\alpha\Delta x\{U_k\})_i^n)$$

DOI: 10.1002/fld

4.2. Numerical approximation of the convective fluxes on moving meshes

We now consider the second integral

$$I_2 = \int_0^{\Delta t}\int_0^{H} ((X_k(F - \dot{x}U))_{i+1/2} - (X_k(F - \dot{x}U))_{i-1/2})\,\mathrm{d}y\,\mathrm{d}t$$
$$= \Delta t H(((\widetilde{X_k(F - \dot{x}U)})_{i+1/2} - (\widetilde{X_k(F - \dot{x}U)})_{i-1/2}))$$

Let us focus on the flux $\int_0^H (X_k(F-\dot{x}U))_{i-1/2}\,\mathrm{d}y$. In order to compute this integral, four instances have to be considered, according to the locations of the fluids in contact at the cell boundary (see Figure 2). Consider, for example, the computation of this integral for phase 1. The contact surfaces for each pair of fluids at the cell boundary are unchanged compared to the previous situation with fixed meshes. Differences appear in the fluxes and phase function sampling. Indeed, since the cell is moving, the fluxes and phase function have to be sampled along the trajectory $x/t = \dot{x}_{i-1/2}$.

Consider, for example, the instance where fluid 1 of cell $(i-1)$ is on the left and fluid 1 of cell (i) is on the right. The indicator function X_1 is always equal to 1 for this type of contact. The flux $(F - \dot{x}_{i-1/2}U)^*_{11}$ is solution of the Riemann problem with fluid 1 on both sides. The flux F and vector of conservative variables U are sampled along the cell boundary trajectory $x/t = \dot{x}_{i-1/2}$.

On another part on the cell boundary $(i-1/2)$, fluid 1 on the left is in contact with fluid 2 on the right. The corresponding flux $(F - \dot{x}_{i-1/2}U)^*_{12}$ is solution of the Riemann problem of the Euler equations with fluid 1 on the left and fluid 2 on the right and is sampled along the same trajectory. We also have to determine the indicator function for this contact at the cell boundary. The interface between 1 and 2 may enter into cell (i) or leave it. When it enters into the cell, the convective fluxes must be accounted for in the evolution of fluid 1. This appears only when $u^*(1,2) > \dot{x}_{i-1/2}$.

The four cases of contact at the cell boundary $(i-1/2)$ are summarized in Table III.

As given previously, the function $X^*_{1,lm}$ represents the fluid indicator function at the cell boundary, where fluid l is initially on the left of the cell boundary and fluid m on the right. When fluid 'l' is in contact with fluid 'm', the indicator function at the cell boundary depends on the sign of the interface velocity. The interface velocity u^*_{lm} is determined by solving the Riemann problem

Table III. The various flow patterns at the left cell boundary and the different ingredients for the flux computation of fluid '1'.

Contact	Surface	Intercell flux sampled along $x/t = \dot{x}_{i-1/2}$	Phase function X^*_1
1–1	S_{11}	$(F - \dot{x}_{i-1/2}U)^*_{11}$	$X^*_{1,11} = 1$
1–2	S_{12}	$(F - \dot{x}_{i-1/2}U)^*_{12}$	$X^*_{1,12} = \begin{cases} 1 & \text{if } u^*(1,2) > \dot{x}_{i-1/2} \\ 0 & \text{otherwise} \end{cases}$
2–1	S_{21}	$(F - \dot{x}_{i-1/2}U)^*_{21}$	$X^*_{1,21} = \begin{cases} 1 & \text{if } u^*(2,1) < \dot{x}_{i-1/2} \\ 0 & \text{otherwise} \end{cases}$
2–2	S_{22}	$(F - \dot{x}_{i-1/2}U)^*_{22}$	$X^*_{1,22} = 0$

Note: The asterisk represents the Riemann problem solution.

DOI: 10.1002/fld

between the two fluids in contact. We define the flux F^*_{lm} and the vector of conservative variables U^*_{lm} solution of the Riemann problem with states l on the left and m on the right of the initial discontinuity. The flux and conservative variables vector are also determined with the help of a Riemann solver. The solution is sampled along the cell boundary trajectory. The length of contact corresponds to the height of contact between fluids at the cell boundary for the flow pattern (l, m). It can be easily checked that the sum of these four lengths corresponds to the total height H.

By summing the four fluxes weighted by the corresponding length and phase function, we get the total flux for fluid '1' at the cell boundary $(i-1/2)$:

$$\int_0^H (X(F-\dot{x}U))_{k,i-1/2}\,\mathrm{d}y = \sum_{l,m} (SX^*_k(F-\dot{x}U)^*)_{lm,i-1/2}$$

Consequently, integral I_2 reads

$$I_2 = \Delta t \left(\sum_{l,m} (SX^*_k(F-\dot{x}U)^*)_{lm,i+1/2} - \sum_{l,m} (SX^*_k(F-\dot{x}U)^*)_{lm,i-1/2} \right)$$

It remains to determine the numerical approximation of integral I_3:

$$I_3 = \int_0^{\Delta t}\int_{x_{i-1/2}}^{x_{i+1/2}} ((X_kG_k)_{y=H} - (X_kG_k)_{y=0})\,\mathrm{d}x\,\mathrm{d}t = 0$$

This integral vanishes again because of wall boundary conditions and the symmetry of the two-phase flow topology.

4.3. Numerical approximation of the non-conservative terms

Following the same guide as previously, we first consider the integral I_4:

$$I_4 = \int_0^{\Delta t}\int_{C_i(t)} (F-\sigma_x U)\frac{\partial X_k}{\partial x}\,\mathrm{d}x\,\mathrm{d}y\,\mathrm{d}t$$

Let us first note that $\partial X_k/\partial x$ is zero everywhere except at the interfaces where it is the Dirac function. The product $(F-\sigma_x U)\partial X_k/\partial x$ is consequently non-zero only at the interfaces. In these locations, since mass transfer is not considered, the interface and fluid velocities are equals $\sigma_x = u$ and the difference $(F-\sigma_x U)$ represents the Lagrangian flux ($F^{\mathrm{lag}} = F-\sigma_x U$). The key remark for the numerical approximation of the non-conservative terms for two-phase flows is that the Lagrangian flux is always constant across the interface, that is at each location where $\partial X_k/\partial x$ is non-zero. Indeed, the Lagrangian flux is only composed of the normal interface velocity (here the velocity along the x-axis) and the pressure. These two variables are precisely constant across the interface. This remark renders possible the integration of $(F-\sigma_x U)\partial X_k/\partial x$.

Second, as shown in Figure 1 there are at most six internal interfaces inside the two-phase control volume C_i. The first four interfaces come from the right and left cell boundaries, while the last two interfaces correspond to the horizontal fluid layer inside the cell. When considering the integral I_4 the term associated with the horizontal interfaces cancels because $\partial X_k/\partial x = 0$. Only the four vertical interfaces must be considered. Thus, we have to determine

$$I_4 = \int_0^{\Delta t} \left(\int_0^H F^{\mathrm{lag}}_{i-1/2}[X^x_k]_{i-1/2}\,\mathrm{d}y + \int_0^H F^{\mathrm{lag}}_{i+1/2}[X^x_k]_{i+1/2}\,\mathrm{d}y \right) \mathrm{d}t$$

DOI: 10.1002/fld

Table IV. The various configurations for Lagrangian fluxes at the left cell boundary.

Contact	Surface	Lagrangian flux	Jump $[X_1^x]^*$
1–1	S_{11}	$F_{11}^{\text{lag},*}$	0
1–2	S_{12}	$F_{12}^{\text{lag},*}$	$[X_1]_{12}^* = \begin{cases} -1 & \text{if } u_{12}^* > \dot{x}_{i-1/2} \\ 0 & \text{otherwise} \end{cases}$
2–1	S_{21}	$F_{21}^{\text{lag},*}$	$[X_1]_{21}^* = \begin{cases} 1 & \text{if } u_{21}^* > \dot{x}_{i-1/2} \\ 0 & \text{otherwise} \end{cases}$
2–2	S_{22}	$F_{22}^{\text{lag},*}$	0

where $[X_k^x] = X_{k,\text{R}} - X_{k,\text{L}}$ represents the jump of the characteristic function between a right (R) and a left (L) state along the x-direction. By using the definition of the averages (7), this last relation can be rewritten as

$$I_4 = \Delta t\, H((\widetilde{F^{\text{lag}}[X_k^x]})_{i-1/2} + (\widetilde{F^{\text{lag}}[X_k^x]})_{i+1/2})$$

We detail the integral calculation for the interfaces coming from the left cell boundary. The same four possible cases that have been considered for the flux computation are summarized in Table IV.

By summing the various terms of Table IV for both cell boundaries and assuming that Lagrangian fluxes are constant during a time step, we have

$$I_4 = \Delta t \left(\sum_{l,m} (SF^{\text{lag},*}[X_k^{x,*}])_{lm,i-1/2} + \sum_{l,m} (SF^{\text{lag},*}[X_k^{x,*}])_{lm,i+1/2} \right)$$

It remains to determine the numerical approximation of the last integral I_5

$$I_5 = \int_0^{\Delta t} \int_{C_i} G^{\text{lag}} \frac{\partial X_k}{\partial y}\, \mathrm{d}x\, \mathrm{d}y\, \mathrm{d}t = \int_0^{\Delta t} \int_{x_{i-1/2}(t)}^{x_{i+1/2}(t)} \sum G^{\text{lag}}[X_k^y]\, \mathrm{d}x\, \mathrm{d}t$$

The jump $[X_k^y]$ is non-zero only for the horizontal interfaces (see Figure 1). The symbol $\sum$ represents the summation over the two horizontal interfaces. The bounds of the space integral are function of time. During the time step the right cell boundary trajectory reads $x_{i+1/2}(t) = \dot{x_{i+1/2}} t + x_{i+1/2}^n$. The term $G^{\text{lag}}[X_k]$ being constant during the time step, the approximation of I_5 reads

$$I_5^{(1)} = \frac{\Delta t}{2} (\Delta x^{n+1} + \Delta x^n)_i (G^{\text{lag},*}{}_i(2,1) - G^{\text{lag},*}{}_i(1,2))$$

$$I_5^{(2)} = -\frac{\Delta t}{2} (\Delta x^{n+1} + \Delta x^n)_i (G^{\text{lag},*}{}_i(2,1) - G^{\text{lag},*}{}_i(1,2))$$

where the superscripts denotes the phase index.

DOI: 10.1002/fld

4.4. Summary of the numerical scheme for moving meshes

Each integral $I_1, \ldots, I_5$ is now divided by $\Delta t \cdot H$. The discretization of (9) for the geometrical description of the two-phase mixture in accordance with Figure 1 is

$$\frac{(\alpha_k \Delta x\{U_k\})_i^{n+1} - (\alpha_k \Delta x\{U_k\})_i^n}{\Delta t} + (\widetilde{\overline{X_k(F - \dot{x}U)}})_{i+1/2} - (\widetilde{\overline{X_k(F - \dot{x}U)}})_{i-1/2}$$
$$= (\widetilde{\overline{F^{\text{lag}}[X_k^x]}})_{i-1/2} + (\widetilde{\overline{F^{\text{lag}}[X_k^x]}})_{i+1/2} + \frac{1}{2}\frac{(\Delta x^{n+1} + \Delta x^n)_i (G^{\text{lag},*}{}_i(k', k) - G^{\text{lag},*}{}_i(k, k'))}{H} \tag{10}$$

The two-phase fluxes read

$$(\widetilde{\overline{X_k(F - \dot{x}U)}})_{i\pm 1/2} = \frac{1}{H}\sum_{l,m} (SX_k^*(F - \dot{x}U)^*)_{lm,i\pm 1/2}$$

And the non-conservative terms read

$$(\widetilde{\overline{F^{\text{lag}}[X_k^x]}})_{i\pm 1/2} = \frac{1}{H}\sum_{l,m} (SF^{\text{lag},*}[X_k^{x,*}])_{lm,i\pm 1/2}$$

In these formulae, the notation (l, m) denotes the flow pattern when the fluid l is on the left and m on the right. The superscript '*' denotes the Riemann problem solution. The definitions of the contact surfaces, fluxes and phase functions are given in Tables III and IV. System (10) is the discrete analogue of System (1). The continuous limit of (10) has been determined when both Δt and Δx tend to zero, in the case of non-moving meshes. The details are given in [12] and provide precisely the system presented initially (1). For another flow topology, a similar limit is obtained in Chinnayya *et al.* [13].

To use numerical scheme (10) the cell boundary velocities have to be determined. This issue is addressed in the next section.

5. LAGRANGIAN CELL BOUNDARIES VELOCITIES

Numerical scheme (10) is an ALE scheme for two-phase flows. In this context, the choice of cells boundaries velocities is arbitrary. However, most applications mentioned in the Introduction involve Lagrangian resolution of the flow field. Since the present model contains three averaged velocities u_1, u_2 and u_I the choice of the Lagrangian velocity $\dot{x}_{i\pm 1/2}$ is not obvious.

Most Lagrangian codes use a continuum fluid model with a single velocity. The continuum model is a system of conservation laws from which the cell boundaries velocities are obtained as solution of the Riemann problem. In the context of multiphase mixtures, the cell boundary velocity can be determined by following a similar approach because additional conservation laws are available for the mixture. These conservation laws are simply obtained by summing the mass,

DOI: 10.1002/fld

momentum and energy equations of both phases. The system obtained from (1) reads

$$\begin{gathered}\frac{\partial(\alpha_1\rho_1+\alpha_2\rho_2)}{\partial t}+\frac{\partial(\alpha_1\rho_1u_1+\alpha_2\rho_2u_2)}{\partial x}=0\\ \frac{\partial(\alpha_1\rho_1u_1+\alpha_2\rho_2u_2)}{\partial t}+\frac{\partial(\alpha_1\rho_1u_1^2+\alpha_2\rho_2u_2^2+\alpha_1P_1+\alpha_2P_2)}{\partial x}=0\\ \frac{\partial(\alpha_1\rho_1E_1+\alpha_2\rho_2E_2)}{\partial t}+\frac{\partial(\alpha_1\rho_1E_1u_1+\alpha_2\rho_2E_2u_2+\alpha_1P_1u_1+\alpha_2P_2u_2)}{\partial x}=0\end{gathered}\tag{11}$$

The Riemann problem solution (or part of it) for this system will provide the mixture velocity at the cell boundaries. This mixture velocity corresponds to the velocity of the centre of mass and is the analogue of the one used with homogeneous fluid models. Thus, the Lagrangian motion of the cell boundaries will be done with this mixture velocity. Its practical determination is detailed hereafter.

Let us recall that the original System (1) involves seven characteristic wave speeds: $\lambda_0^1=u_1$, $\lambda_1^1=u_1-c_1$, $\lambda_2^1=u_1+c_1$, $\lambda_0^2=u_2$, $\lambda_1^2=u_2-c_2$, $\lambda_2^2=u_2+c_2$ and $\lambda_I=u_I$. System (11) involves the same wave speeds. To determine the mixture velocity at the cell boundary $(i-1/2)$ separating cell $(i-1)$ on the left and cell (i) on the right, we adopt an approximate resolution of the Riemann problem for System (11). The HLL strategy [24] is adopted and is accurate enough since only the mixture velocity is required. Within the HLL solver, only the fastest right- and left-facing wave speeds are necessary. We denote by S_R the right-facing wave speed and by S_L the left-facing one. Following Davis [25] these wave speeds may be estimated as

$$S_R=\mathrm{Max}(0;\lambda_{2,i-1}^1;\lambda_{2,i}^1;\lambda_{2,i-1}^2;\lambda_{2,i}^2),\quad S_L=\mathrm{Min}(0;\lambda_{1,i-1}^1;\lambda_{1,i}^1;\lambda_{1,i-1}^2;\lambda_{1,i}^2)$$

Let us now write System (11) under reduced form

$$\frac{\partial U_{\mathrm{mix}}}{\partial t}+\frac{\partial F_{\mathrm{mix}}}{\partial x}=0$$

with the conservative vector of variables

$$U_{\mathrm{mix}}=((\alpha_1\rho_1+\alpha_2\rho_2),(\alpha_1\rho_1u_1+\alpha_2\rho_2u_2),(\alpha_1\rho_1E_1+\alpha_2\rho_2E_2))^{\mathrm{T}}$$

and the associated conservative flux vector.

With these notations, the vector of conservative variables at the cell boundary $(i-1/2)$, under HLL approximation, reads

$$U_{\mathrm{mix},i-1/2}^{\mathrm{HLL}}=\frac{S_RU_{\mathrm{mix},i}-S_LU_{\mathrm{mix},i-1}+F_{\mathrm{mix},i-1}-F_{\mathrm{mix},i}}{S_R-S_L}$$

Thus, the boundary cell velocity is easily determined as the ratio of the second and first components of this vector:

$$\dot{x}_{i-1/2}=\frac{S_RU_{\mathrm{mix},i}^{(2)}-S_LU_{\mathrm{mix},i-1}^{(2)}+F_{\mathrm{mix},i-1}^{(2)}-F_{\mathrm{mix},i}^{(2)}}{S_RU_{\mathrm{mix},i}^{(1)}-S_LU_{\mathrm{mix},i-1}^{(1)}+F_{\mathrm{mix},i-1}^{(1)}-F_{\mathrm{mix},i}^{(1)}}\tag{12}$$

where the superscripts (1) and (2) denote the components of vectors U_{mix} and F_{mix}.

DOI: 10.1002/fld

With the help of Formula (12), the Riemann problem solution sampling is possible. The cells size evolution is also obtained with the cells boundary velocities as

$$\Delta x_i^{n+1} = \Delta x_i^n + \Delta t\,(\dot{x}_{i+1/2} - \dot{x}_{i-1/2})$$

All formulae are now available and numerical tests can be done. Let us just mention that this scheme is stable under conventional CFL restriction based on the fastest wave speed.

6. NUMERICAL TESTS

The Lagrangian numerical method is validated over different tests involving interfaces, shocks and relaxation effects.

6.1. Uniform velocity and pressure flow with a volume fraction discontinuity

We consider a tube filled with a two-phase mixture. Both phases are in velocity and pressure equilibrium. Moreover, the flow velocity, as well as the pressure is uniform in the entire tube. At the centre a volume fraction discontinuity separates a mixture on the left that contains mainly a heavy fluid with a polytropic exponent of 3 from another mixture on the right that contains mainly a light gas with a polytropic exponent of 1.4. This test has a trivial solution corresponding to the pure advection of the volume fraction discontinuity. However, it presents two interesting features:

- The two-phase algorithm being quite complex, it is important to check that it fulfils this basic test. Note that in the context of a pure Eulerian scheme, this test presents an important difficulty related to the smearing of the volume fraction wave, responsible for the apparition of an artificial mixture zone, for which the computation of the pressure, sound speed, temperature and in fact all thermodynamic variables pose difficulties. This issue has been addressed by many authors [6, 11, 26–31] with various types of modelling approaches and numerical schemes. We will check that the present algorithm does not create any spurious pressure or velocity oscillation with both Eulerian and Lagrangian formulations.
- The Eulerian and Lagrangian solutions will be compared in order to illustrate their differences for the capturing of volume fraction waves.

Each fluid is governed by the ideal gas equation of state: $P_k = (\gamma_k - 1)\rho_k e_k$ with $\gamma_1 = 3$ and $\gamma_2 = 1.4$. The heavy fluid (phase 1) is present initially everywhere with the density $\rho_1 = 100\,\mathrm{kg/m^3}$ but with different volume fractions. The light gas (phase 2) is also present everywhere with the density $\rho_2 = 1\,\mathrm{kg/m^3}$. Both phases velocities are uniform ($u = 100\,\mathrm{m/s}$) as well as initial pressures ($P = 10^5\,\mathrm{Pa}$). On the left of the tube ($x < 0.5\,\mathrm{m}$), the heavy fluid volume fraction is $\alpha_1 = 1 - \varepsilon$ while on the right part of the tube it is $\alpha_1 = \varepsilon$ with $\varepsilon = 10^{-6}$. Since the two chambers contain nearly pure fluids, a heavy one on the left and a light one on the right, the numerical solution can be compared to the one obtained with the Euler equations with a contact discontinuity separating the two gases. The solutions are shown at time 1703 μs in Figure 3. The exact solution is shown with lines while the numerical ones are shown with symbols.

On the left part of Figure 3 the numerical solution obtained with the Lagrangian scheme is compared with the exact solution. On the right part, the same comparison is done with the Eulerian version. Both numerical computations are done with a mesh involving 100 cells. It appears clearly

DOI: 10.1002/fld

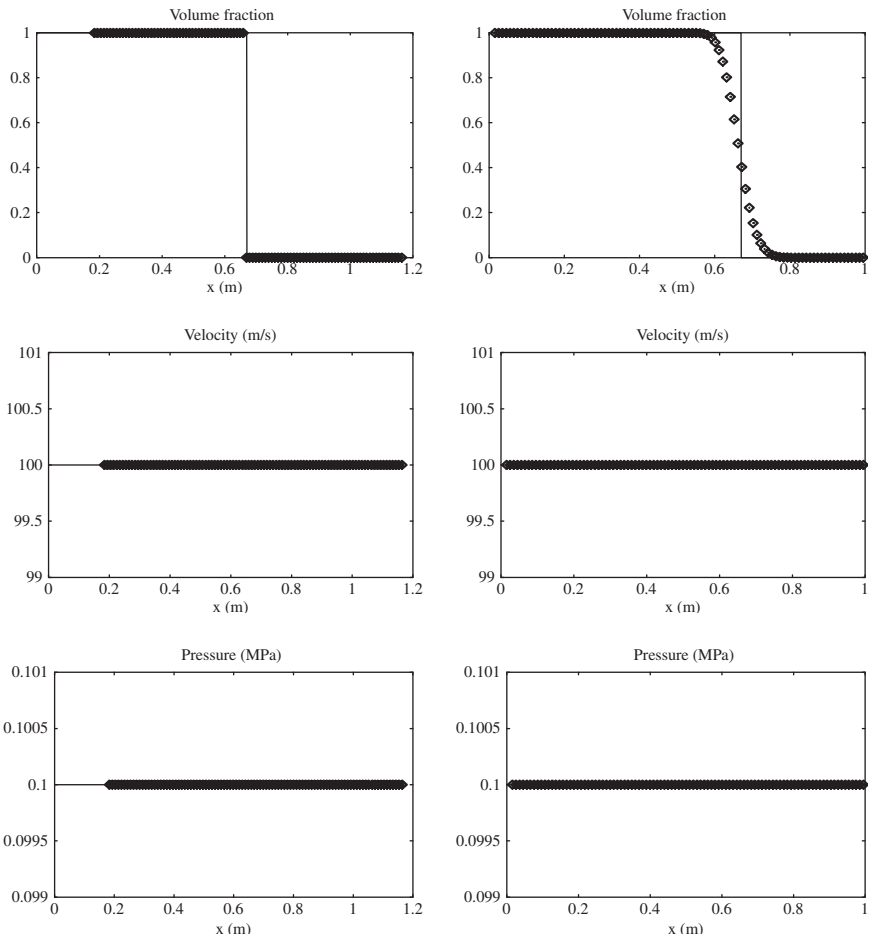

Figure 3. Propagation of an interface/volume fraction discontinuity in a uniform velocity and pressure flow. The exact solution is shown with lines and the numerical one is shown with symbols. The left graphs correspond to the Lagrangian method and those on the right correspond to the Eulerian version.

that both methods preserve perfectly the uniform velocity and pressure flow conditions. Positivity of the volume fraction is also obtained. The Lagrangian method shows a better representation of the volume fraction discontinuity, as was expected.

6.2. Shock tube test problems

We consider a shock tube filled on the left side with a high-pressure heavy fluid and on the right side with a light gas at lower pressure. This test problem consists of a conventional shock tube with two fluids and has an exact solution. Since the two fluids are pure, only separated by an interface, the Riemann problem of the Euler equations provides the exact solution. However, it is well known [27] that the numerical solution of the Euler equations produces spurious pressure and velocity oscillations when the polytropic coefficients are discontinuous. The multiphase model is

DOI: 10.1002/fld

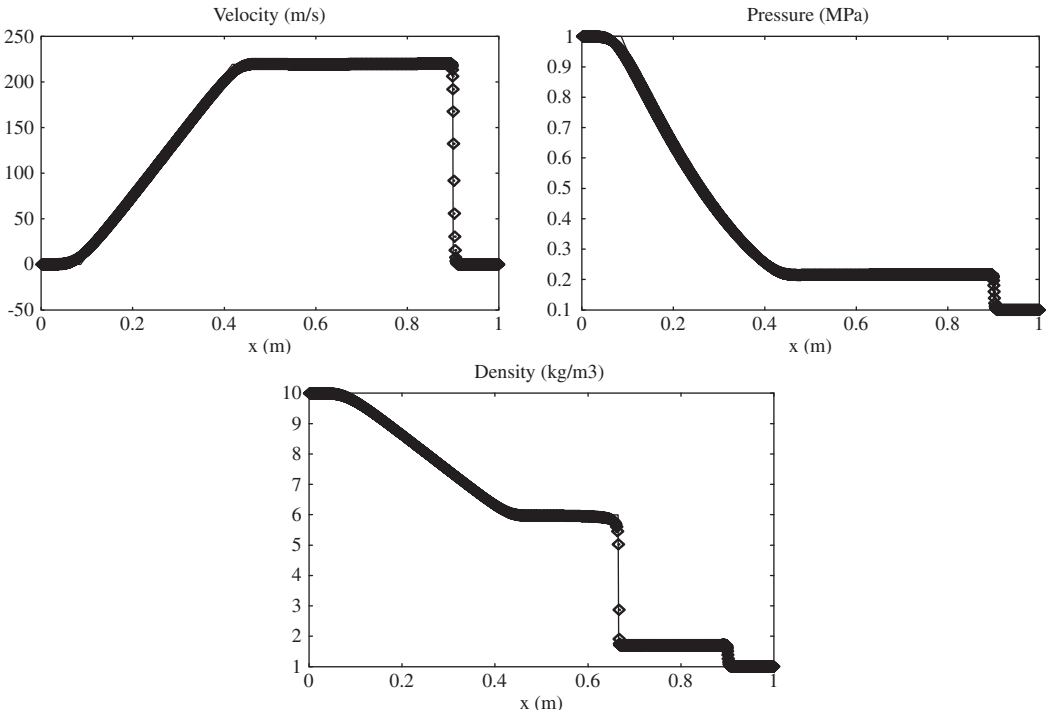

Figure 4. Shock tube with an interface separating nearly pure fluids. The Lagrangian scheme is used. The exact solution is shown with lines and the numerical one with symbols.

able to cure this problem, as shown in this example. We retain the same equation of state and polytropic exponents as in the previous test ($\gamma_1 = 3$ for the heavy fluid and $\gamma_2 = 1.4$ for the light fluid). The heavy fluid is initially present everywhere with the density $\rho_1 = 10\,\mathrm{kg/m^3}$ but with different volume fractions. The light gas (phase 2) is also present everywhere with the density $\rho_2 = 1\,\mathrm{kg/m^3}$. Both phases are initially at rest $u = 0\,\mathrm{m/s}$. On the left of the tube ($x < 0.5\,\mathrm{m}$), the heavy fluid volume fraction is $\alpha_1 = 1 - \varepsilon$ with the initial pressure of $P = 10^6\,\mathrm{Pa}$ and on the right part of the tube its volume fraction is $\alpha_1 = \varepsilon$ with $\varepsilon = 10^{-6}$ and initial pressure $P = 10^5\,\mathrm{Pa}$. The solutions are shown at time 755 μs in Figure 4. The exact solution is shown with lines while the numerical one is shown with symbols. To show mesh convergence of the results, a mesh involving 1000 cells is used. The fluids densities and internal energies are not compared with the exact solution because no exact solution exists for these variables (no exact Riemann solver is available for this model). Only the mixture density ($\rho_{\mathrm{mix}} = \alpha_1\rho_1 + \alpha_2\rho_2$), pressure ($P_{\mathrm{mix}} = \alpha_1 P_1 + \alpha_2 P_2$) and velocity ($u_{\mathrm{mix}} = (\alpha_1\rho_1 u_1 + \alpha_2\rho_2 u_2)/(\alpha_1\rho_1 + \alpha_2\rho_2)$) can be compared with the exact solution. Excellent agreement is obtained. The test problems of Figures 3 and 4 clearly show that the method is able to deal with interface problems. We now consider flows of two-phase mixtures with several velocities.

We reuse the same initial conditions as previously, except that the initial volume fraction is 0.5 everywhere. It means that the diaphragm separates the high-pressure chamber and the low-pressure one, and that both chambers contain a mixture of two fluids, a heavy one and a light one, with

DOI: 10.1002/fld

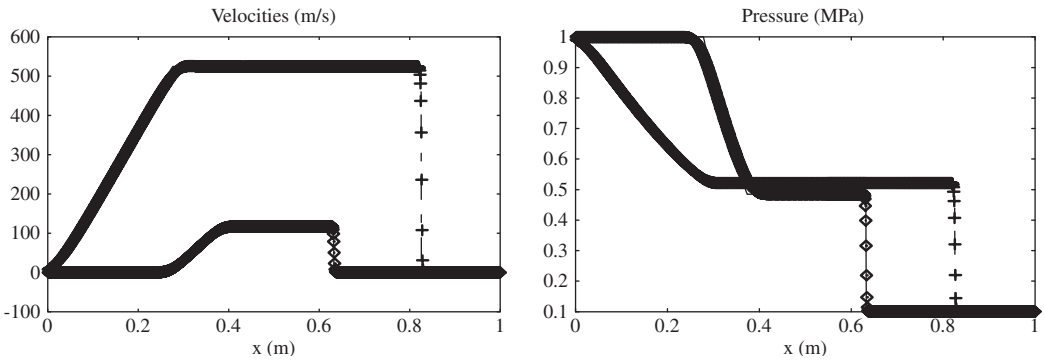

Figure 5. Shock tube with a mixture of heavy and light fluids. Pressure and velocity relaxation effects are removed. The numerical solution obtained with the Lagrangian scheme is shown with symbols. The exact solution is shown with lines. The single-phase behaviour of the Euler equations is recovered.

different equations of state. Since the two fluids behave with their own equation of state and have different densities, they will behave with different velocities. In this test problem, the relaxation parameters μ and λ are set to zero in System (1). In the discrete approximation, corresponding relaxation terms ($\sum G^{\text{lag}}[X^y]$) are set to zero. It means that no interaction exists between the fluids. As the volume fraction is initially uniform and that no pressure relaxation effects are accounted for, the volume fraction will remain uniform. Thus, each pure fluid behaves as if it was alone and the multiphase flow solution can be compared to the one of the Euler equations, solved two times. The solutions are shown at time 405 μs in Figure 5. The fluid having the fastest flow velocity as well as the fastest shock wave corresponds to the light one. These results show clearly that the Lagrangian scheme behaves correctly for fluid mixtures where each component has its own velocity. To investigate a little more the effects related to pressure relaxation, let us consider the same test problem where now the term $\sum G^{\text{lag}}[X^y]$ is activated. In this term, the parameter related to the tube height has been taken equal to 3 mm: $H = 0.003$ m. It results in stiff pressure and velocity relaxation effects. The results are displayed in Figure 6 at time 473 μs. Again, the results are obtained with a mesh involving 1000 cells, but no comparison with an exact solution is available. The variables of fluid 1 are shown with lines while those of fluid 2 are shown with symbols. The results clearly show that at relaxed state both pressures and velocities are equal. These relaxation processes involve volume fraction variations across the various waves.

6.3. Shock bubble interaction test problem

We now consider a more difficult test problem given in full detail in Saurel *et al.* [12]. It consists in the study of the two-dimensional interaction of a shock wave propagating in a heavy gas, with the same characteristics as the one used before, with a light gas bubble having also the same characteristics as in the previous tests. The initial situation is depicted in Figure 7.

When the shock interacts with the light gas bubble, the interface undergoes a complex motion resulting in the bubble contraction and fluid rotation. In order to account for turbulent motion with a one-dimensional model, extra terms have to be added to System (1). Turbulent pressure, energy effects can be added to the equations without changing the general structure. An extra equation

DOI: 10.1002/fld

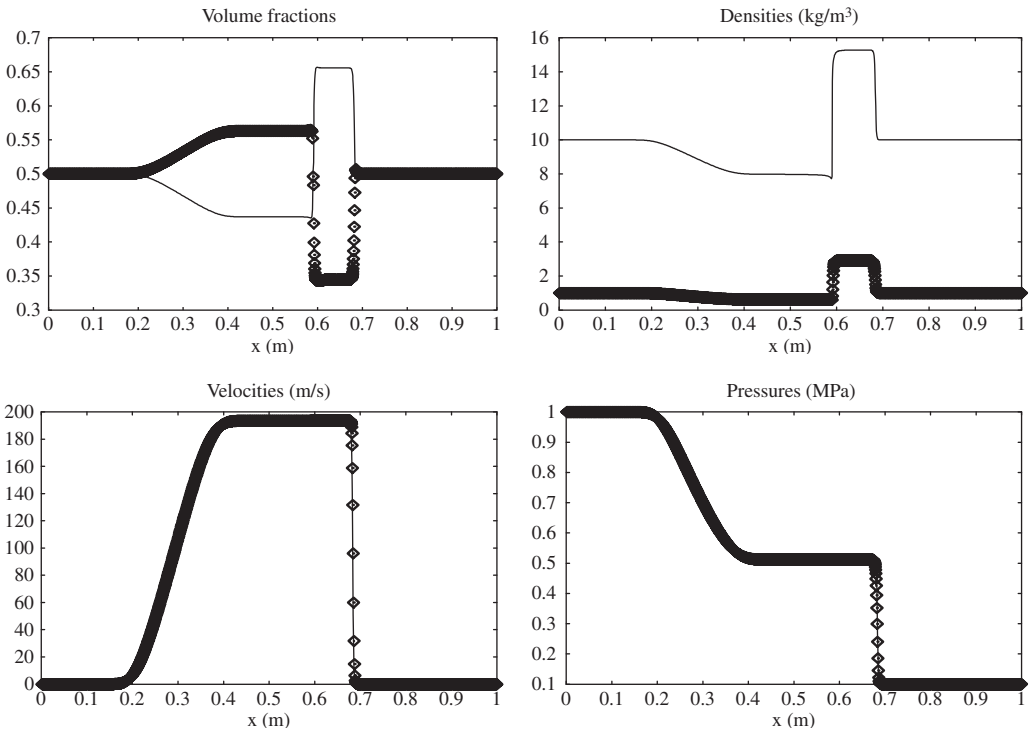

Figure 6. Shock tube with two mixtures of heavy and light fluids. The pressure and velocity relaxation terms are used. The numerical solution obtained with the Lagrangian scheme is shown with symbols for the light fluid and with lines for the heavy one. The relaxed pressure and velocity states are obtained through the shock and rarefaction waves.

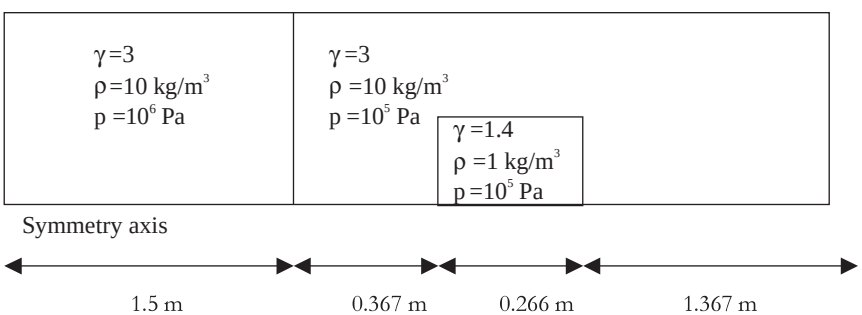

Figure 7. Schematic representation of a shock tube containing a heavy gas and a light gas bubble.

is necessary to account for the turbulent entropy transport. Creation terms are present to model turbulence creation in the shock relaxation zone. The extension of the two-phase flow model to such turbulent effects is summarized in System (13). The details regarding the derivation are given

DOI: 10.1002/fld

in Saurel *et al.* [12]

$$
\begin{aligned}
\frac{\partial \alpha_1}{\partial t} + u_{\mathrm{I}} \frac{\partial \alpha_1}{\partial x} &= \mu(P_1 - P_2) \\
\frac{\partial \alpha_1 \rho_1}{\partial t} + \frac{\partial (\alpha_1 \rho_1 u_1)}{\partial x} &= 0 \\
\frac{\partial \alpha_1 \rho_1 u_1}{\partial t} + \frac{\partial (\alpha_1 \rho_1 u_1^2 + \alpha_1 P_1)}{\partial x} &= P_{\mathrm{I}} \frac{\partial \alpha_1}{\partial x} + \lambda(u_2 - u_1) \\
\frac{\partial \alpha_1 \rho_1 E_1}{\partial t} + \frac{\partial (\alpha_1 \rho_1 E_1 u_1 + \alpha_1 P_1 u_1)}{\partial x} &= P_{\mathrm{I}} u_{\mathrm{I}} \frac{\partial \alpha_1}{\partial x} - \mu P'_{\mathrm{I}}(P_1 - P_2) + \lambda u'_{\mathrm{I}}(u_2 - u_1) \\
\frac{\partial \alpha_1 \rho_1 s_{t1}}{\partial t} + \frac{\partial \left(\alpha_1 \rho_1 s_{t1} u_1\right)}{\partial x} &= \frac{Z_1}{T_{t1}(Z_1 + Z_2)} \left(\left((P_2 - P_1) + \mathrm{sgn}\left(\frac{\partial \alpha_1}{\partial x}\right) \right. \right. \\
&\qquad \left. \left. \times\ (u_2 - u_1) Z_2 \right)^2 \left| \frac{\partial \alpha_1}{\partial x} \right| + \mu (P_2 - P_1)^2 \right)
\end{aligned}
\tag{13}
$$

System 13 is aimed to reduce multidimensional effects in a one-dimensional model. These multidimensional effects are expressed through two transport velocities, one collapse velocity and two rotation velocities. The first effects were already present in System 1. Rotation or turbulent effects have been added at the scale of the light gas bubble. In System 13 the last equation expresses the evolution of the turbulent entropy s_{tk} of fluid k. Following Saurel *et al.* [32] it is connected to the turbulent energy and turbulent pressure through the relations: $\mathrm{e}_{tk} = (1/(\gamma_{\mathrm{t}} - 1))\rho^{\gamma_{\mathrm{t}}-1} \exp(s_{tk}/C v_{tk})$ and $p_{tk} = (\gamma_{\mathrm{t}} - 1)\rho \mathrm{e}_{tk}$. The polytropic turbulent exponent γ_{t} is equal to $\frac{5}{3}$ when the vortices evolve in three dimension and is equal to 2 when they evolve in two dimension. The 'specific heat' of vortices is given by $C v_{tk} = R_k/(\gamma_{\mathrm{t}} - 1)$. From these definitions, the turbulent temperature T_{tk} appearing in the right-hand side of the last equation of (13) reads $T_{tk} = \mathrm{e}_{tk}/C v_{tk}$. The right-hand side of this equation represents the turbulent entropy creation term. It models the turbulence creation at each interface of the multiphase mixture.

In this system, the total pressure P_k is the sum of two terms: the thermodynamic pressure p_k and the turbulent pressure p_{tk}. Thus, the total pressure reads $P_k = p_k + p_{tk}$. The same remarks holds for the total energy, that is the sum of three terms: $E_k = \mathrm{e}_k + \mathrm{e}_{tk} + \frac{1}{2}u_k^2$. The square of the sound speed in each phase is also the sum of two terms $C_k^2 = c_k^2 + c_{tk}^2$ where the turbulent sound speed expresses $c_{tk}^2 = \gamma_{\mathrm{t}} p_{tk}/\rho_k$. The thermodynamic speed of sound c_k is conventional.

This last remark implies that all closure formulae for P_{I}, P'_{I}, u_{I}, u'_{I}, λ and μ are still valid, except that the acoustic impedance Z_k now uses the total sound speed C_k. It is noticeable that the one-dimensional model does not involve any parameter. All terms of System (13) have explicit expressions.

This turbulent two-phase flow model can be easily shown as unconditionally hyperbolic.

In order to validate this model, reference results are necessary. They are obtained by two-dimensional direct numerical simulation of the flow situation shown in Figure 7. An interface being present, an appropriate model and numerical algorithm has to be employed. We have used a method based on a reduced multiphase flow model with single pressure and velocity able to deal

DOI: 10.1002/fld

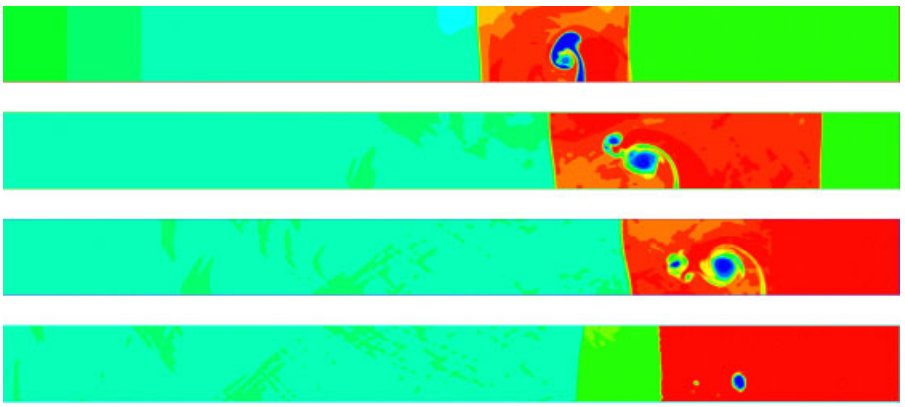

Figure 8. Computed density contours for the shock/bulle interaction problem at times 2.91, 5.24, 7.66 and 9.66 ms (top–down). The bubble contraction as well as its rotational motion is clearly visible.

with interfaces and large deformations [30]. To give an illustration of the unsteady phenomena under study, the density contours at times 2.91, 5.24, 7.66 and 9.66 ms are shown in Figure 8. These results correspond to the reference solution that will be used to validate the one-dimensional turbulent multiphase flow model. In order to compare one-dimensional and two-dimensional computations, the two-dimensional results are averaged over each cross section.

The averaged two-dimensional results and the multiphase model one-dimensional (13) results, solved with the Lagrangian scheme are shown in Figure 9. During shock–bubble interaction rotation (turbulent) effects appear and result in turbulent entropy, turbulent energy and turbulent pressure increase. Since the interface conditions between the bubble and the surrounding fluid have to be fulfilled, the total pressure has to be constant across the interface. It results in a thermodynamic pressure decrease in the gas bubble, as shown in Figure 9.

Both numerical simulations (one- and two-dimensional) are done with a mesh involving 1000 cells in the x-direction. The two-dimensional mesh uses 90 cells in the y-direction. The comparison in Figure 9 shows an excellent agreement. The only flow variable where the agreement is perfectible is the volume fraction at time 5.24 ms. The reason is that the interface has a multi-valuated velocity in two dimensions, while it has been considered in one dimension as single valued. This modelling issue will be addressed in the future.

7. CONCLUSION

An efficient Lagrangian numerical scheme has been developed for a multiphase models involving phases compressibility. The scheme building follows the discrete approach of Abgrall and Saurel [11], Saurel *et al.* [12], Chinnayya *et al.* [13] and LeMetayer *et al.* [14]. The various fluxes are upwinded by considering all waves present in the flow model. The non-conservative terms are approximated correctly in the presence of volume fraction discontinuities and as well as shocks. These issues are addressed in the context of moving meshes. The cells boundaries velocities are determined with an approximate Riemann solver for the complementary conservation laws of the non-conservative model. Several test problems with growing level of difficulty are solved.

DOI: 10.1002/fld

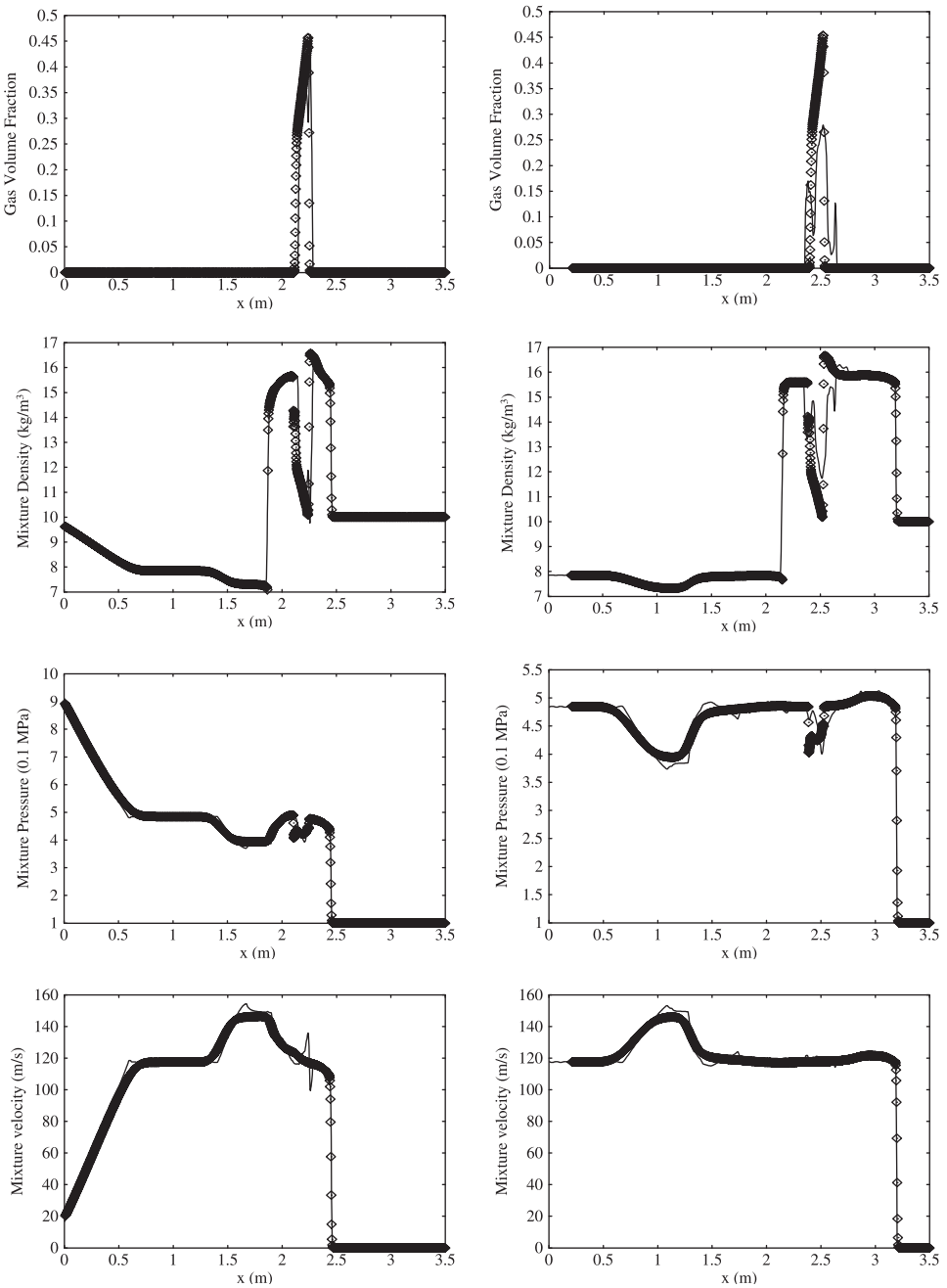

Figure 9. Comparison of the one-dimensional model predictions (symbols) *versus* the two-dimensional averaged results (lines). The left and right column graphs correspond to the time instants 2.91 and 5.24 ms, respectively.

DOI: 10.1002/fld

REFERENCES

1. Stewart H, Wendroff B. Two-phase flow: models and methods. *Journal of Computational Physics* 1984; **56**: 363–409.
2. Baer M, Nunziato J. A two-phase mixture theory for the deflagration-to-detonation transition (DDT) in reactive granular materials. *International Journal of Multiphase Flows* 1986; **12**:861–889.
3. Youngs D. Modeling turbulent mixing by Rayleigh–Taylor instability. *Physica D* 1989; **37**:270–287.
4. Youngs D. Three-dimensional numerical simulation of turbulent mixing by Rayleigh–Taylor instability. *Physics of Fluids* 1989; **A3**:1312–1319.
5. Kapila A, Son S, Bdzil J, Menikoff R, Stewart D. Two-phase modeling of DDT: structure of the velocity-relaxation zone. *Physics of Fluids* 1997; **9**(12):3885–3897.
6. Saurel R, Abgrall R. A multiphase Godunov method for compressible multifluid and multiphase flows. *Journal of Computational Physics* 1999; **150**:425–467.
7. Glimm J, Saltz D, Sharp D. Two-phase modelling of a fluid mixing layer. *Journal of Fluid Mechanics* 1999; **378**:119–143.
8. Kapila A, Menikoff R, Bdzil J, Son S, Stewart D. Two-phase modeling of DDT in granular materials: reduced equations. *Physics of Fluids* 2001; **13**:3002–3024.
9. Saurel R, LeMetayer O. A multiphase model for compressible flows with interfaces, shocks, detonation waves and cavitation. *Journal of Fluid Mechanics* 2001; **431**:239–271.
10. Gavrilyuk S, Saurel R. A compressible multiphase flow model with microinertia. *Journal of Computational Physics* 2002; **175**:326–360.
11. Abgrall R, Saurel R. Discrete equations for physical and numerical compressible multiphase mixtures. *Journal of Computational Physics* 2003; **186**(2):361–396.
12. Saurel R, Gavrilyuk S, Renaud F. A multiphase model with internal degrees of freedom: application to shock-bubble interaction. *Journal of Fluid Mechanics* 2003; **495**:283–321.
13. Chinnayya A, Daniel E, Saurel R. Computation of detonation waves in heterogeneous energetic materials. *Journal of Computational Physics* 2004; **196**:490–538.
14. LeMetayer O, Massoni J, Saurel R. Modeling evaporation fronts with reactive riemann solvers. *Journal of Computational Physics* 2005; **205**:567–610.
15. Benson DJ. Computational methods in Lagrangian and Eulerian hydrocodes. *Computer Methods in Applied Mechanics and Engineering* 1992; **99**:235–394.
16. Yamada S. An implicit Lagrangian code for spherically symmetric general relativistic hydrodynamics with an approximate Riemann solver. *The Astrophysical Journal* 1997; **475**:720–739.
17. Bezard F, Despres B. An entropic solver for ideal Lagrangian magnetohydrodynamics. *Journal of Computational Physics* 1999; **154**(1):65–89.
18. Wilkins M. *Computer Simulation of Dynamics Phenomena*. Springer: Berlin, 1999.
19. Despres B. Lagrangian systems of conservation laws and approximate Riemann solvers. In *Godunov Methods, Theory and Applications*, Toro EF (ed.), 2001; 233–246.
20. Anderson RW, NSE, Pember RB. An arbitrary Lagrangian–Eulerian method with adaptive mesh refinement for the solution of the Euler equations. *Journal of Computational Physics* 2004; **199**(2):598–617.
21. Drew D, Passman S. *Theory of Multicomponent Fluids*, *Applied Mathematical Sciences*. vol. 135. Springer: New York, 1998.
22. Hou T, Floch PL. Why non-conservative schemes converge to the wrong solution: error analysis. *Mathematics of Computation* 1994; **62**:497–530.
23. Dalmaso G, Floch PL, Murat F. Definition and weak stability of non-conservative products. *Journal de Mathematiques Pures et Appliquees* 1995; **74**:483–548.
24. Harten A, Lax P, van Leer B. On upstream differencing and Godunov type schemes for hyperbolic conservation laws. *SIAM Review* 1983; **25**:33–61.
25. Davis SF. Simplified second order Godunov type methods. *SIAM Journal on Scientific Computing* 1988; **9**: 445–473.
26. Karni S. Hybrid multifluid algorithms. *SIAM Journal on Scientific Computing* 1996; **17**(5):1019–1039.
27. Abgrall R. How to prevent pressure oscillations in multicomponent flow calculations: a quasi conservative approach. *Journal of Computational Physics* 1996; **125**:150–160.
28. Shyue K. An efficient shock-capturing algorithm for compressible multicomponent problems. *Journal of Computational Physics* 1998; **142**(1):208–242.

DOI: 10.1002/fld

29. Fedkiw R, Aslam T, Merriman B, Osher S. A nonoscillatory Eulerian approach to interfaces in multimaterial flows (The Ghost Fluid Method). *Journal of Computational Physics* 1999; **152**:457–492.
30. Massoni J, Saurel R, Nkonga B, Abgrall R. Proposition de methodes et modeles euleriens pour les problemes a interfaces entre fluides compressibles en presence de transfert de chaleur. *International Journal of Heat and Mass Transfer* 2002; **45**:1287–1307.
31. Allaire G, Clerc S, Kokh S. A five-equation model for the simulation of interfaces between compressible fluids. *Journal of Computational Physics* 2002; **181**:577–616.
32. Saurel R, Chinnayya A, Renaud F. Thermodynamic analysis and numerical resolution of a turbulent fully ionised plasma flow model. *Shock Waves* 2003; **13**:283–298.

DOI: 10.1002/fld